

Influence of the bias voltage on the structure and the tribological performance of nanoscale multilayer C/Cr PVD coatings

Y.N. Kok^{a,*}, P.Eh. Hovsepian^a, Q. Luo^a, D.B. Lewis^a, J.G. Wen^b, I. Petrov^b

^aMaterials Research Institute, Sheffield Hallam University, Howard Street, Sheffield S1 1WB, UK

^bMaterials Science Department and Frederick Seitz Materials Research Laboratory, University of Illinois, 1101 West Springfield Avenue, Urbana, IL 61801, USA

Available online 26 October 2004

Abstract

Nanoscale multilayer C/Cr coatings have been deposited by utilising the combined steered cathodic arc/unbalanced magnetron sputtering technique. The coating microstructure and tribological performance have been investigated as a function of the bias voltage, ranging from $U_b = -65$ to -350 V. The XRD results revealed that C/Cr coatings are amorphous at low U_b , but became more crystalline when the U_b increased to -350 V. High-resolution XTEM analysis indicated coating densification and smoothening as well as formation of novel amorphous nanostructure, in which carbon-rich clusters are surrounded by a Cr-rich matrix, leading to the formation of self-organised multilayer structure as the bias voltage was increased from -65 to -350 V. An increase of the bias voltage from -65 to -350 V resulted in an increase in the hardness from 8 to 25 GPa and Young's modulus, E from 186 to 319 GPa. A pin-on-disc test showed that the friction coefficient was reduced from 0.22 to 0.16 when the bias voltage was increased from -65 to -95 V. However, a further increase in the bias voltage to -350 V led to an increase in the friction coefficient to 0.31. The lowest wear coefficient $K_c \sim 6.25 \times 10^{-17} \text{ m}^3 \text{ N}^{-1} \text{ m}^{-1}$ was achieved at $U_b = -120$ V. Standard HSS drills, 8 mm in diameter, coated with C/Cr have been tested using solution annealed AISI 304 stainless steel as the work piece material. An improvement of the lifetime by a factor of ~ 9 has been achieved as compared to the uncoated tools. In this test, the C/Cr coating outperformed a number of commercially available PVD coatings, such as TiCN, TiAlCrN and showed similar performance to TiAlCrYN.

© 2004 Elsevier B.V. All rights reserved.

Keywords: Sputtering; C/Cr coating; Bias voltage; Tribology; Microstructure

1. Introduction

The extensive research in solid lubricant carbon-based coatings arises from the low friction coefficient and low shear strength of the graphite which confers excellent tribological performance in various industrial applications, such as cutting tools, automotive components, precision parts, and bearings [1–4]. It has been suggested that the excellent tribological performance of carbon-based coatings during sliding in ambient atmosphere results from the following factors:

(a) the nature of the sp^2 bonding with weak van der Waals bond between the hexagonal crystallographic structure of graphite,

- (b) low surface energy of the sliding surface and low interlamellar binding energy due to the adsorbed gases (e.g., hydrogen, oxygen, hydroxyl) or water vapour [5–7],
- (c) ability of graphite to form a transfer layer through atomic linkages between the metal and graphite because of the presence of oxides or condensable gases [8],
- (d) wear-induced graphitisation process [9–11], and
- (e) reorientation of the graphite nanocrystallised clusters of the outmost surface (~ 2.5 nm) of the coating which results in planes parallel to the rubbing surface [12].

The tribological performance of carbon-based coatings depends very much on the testing atmosphere and conditions [10,13], the deposition techniques, and the deposition parameters. Of particular importance in this respect is the substrate bias voltage which controls the ion bombardment

* Corresponding author Tel.: +44 114 221 3043; fax: +44 114 221 3053.
E-mail address: y.n.kok@shu.ac.uk (Y.N. Kok).

energy on the growing film and plays a crucial role in determining the properties of the coating. Low energy (~ 25 – 5000 eV) ion irradiation [14] during film growth is known to enhance adatom mobility, control the nucleation and growth kinetics, induce additional stresses, and thus modify the properties, composition, and the structure of the growing thin film [15,16]. It has been speculated that the structure of the sputtered carbon coatings that consists of very fine grains of graphite-like carbon with cross bonding between the graphite-like layers is due to the ion bombardment conditions during sputtering [4]. A recent publication [17] on the metal-doped (i.e., chromium) carbon film has reported that the low friction coefficient of the film was due to the densification and the smoothening caused by ion irradiation effects. However, the effect of ion bombardment on the evolution of the microstructure and on the tribological behaviour of C/Cr coatings has not yet been understood fully.

The aim of this paper is to explain the effects of ion bombardment on microstructural evolution and tribological performance of C/Cr coatings. To achieve this, coatings grown under a wide range of bias voltages, U_b between -65 and -350 V, have been investigated.

2. Experimental procedure and characterisation techniques

C/Cr coatings were deposited by the combined steered cathodic arc/unbalanced magnetron sputtering (ABS™: Arc-Bond Sputtering) technique [18,19] using Hauzer HTC 1000-4 PVD coater. The details of the coating process have been reported previously elsewhere [11,17]. C/Cr coatings were deposited in three major steps: (i) Cr^+ ion etching using a steered cathodic arc discharge at a substrate bias voltage of -1200 V. It has been demonstrated that the metal ion bombardment favours local epitaxial film growth, which enhances adhesion between coating and substrate [20,21]. Additionally, the Cr^+ etching minimises the surface roughness of the subsequent coatings [22]; (ii) deposition of CrN base layer by unbalanced magnetron sputtering to further enhance the adhesion; and (iii) deposition of C/Cr coatings by unbalanced magnetron sputtering from three graphite targets and one chromium target at 260°C . The coatings were deposited at different bias voltages of -65 , -75 , -95 , -120 , and -350 V in nonreactive Ar atmosphere.

The adhesion of the films was evaluated by CSEM REVETEST scratch tester by measuring the critical load of coating failure, L_c . The tribological studies were conducted using a pin-on-disc (CSEM tribometer) apparatus. The tests have been carried out in ambient atmosphere (RH: 13–34%, temperature: 25 – 28°C) under the testing conditions of 5 N normal load, 0.1 ms^{-1} sliding speed, sliding distance of 1.3 km, using a 6-mm 100Cr6 steel ball. The cross-sectional area of the wear track was measured using a laser profilometer, four measurements were taken on each sample at 90° apart. The coating thickness was measured by ball

cratering techniques (CSEM Calotest). The hardness and the Young's modulus, E , of the coating were determined by nanoindentation test (Nano-Instrument XP), by setting the maximum penetration depth to 250 nm; 25 measurements were taken in order to obtain statistical average results. The stress of the coatings was determined by the deflection method using Stoney's equation [23]:

$$\sigma = (E_s d^2) / [6(1 - \nu_s) R d_c]$$

where E , d , ν , and R are the Young's modulus, thickness, Poisson ratio (0.3 was used in the calculation), and the radius of curvature of the coated substrate, respectively; subscripts s and c denote the substrate and the coating, respectively. The coatings for the stress measurement have been deposited on a rectangular steel substrates ($E_s = 260$ GPa) with a dimensions $0.1 \times 10 \times (50 \pm 0.5)$ mm³. The maximum deflection of the coated substrate was measured by optical microscopy (Society Genevoise Optical Measuring Machine). Secondary Neutral Mass Spectrometry [SNMS, quantitative-using certified reference materials (CRM)], VG SIMSLAB was used for the compositional depth profiling of the films.

The structure of C/Cr was investigated by X-ray diffraction (XRD) analysis utilising Philips PW 1710 automated diffractometer, using glancing angle (fix at 1° incidence angle) and $\theta/2\theta$ geometries, scanning from 10° to 100° with a step size of 0.04° . Cross-sectional transmission electron microscopy (XTEM; Philips CM20 operated at 200 kV) and high-resolution TEM (HRTEM; JEOL 2010F operated at 200 kV) were used to study the microstructure of the coatings.

3. Results and discussion

3.1. Compositional analysis

The SNMS depth profiling results showed that for the applied bias voltages in the range of -65 to -120 V, the concentration of carbon and chromium in the films remained constant at ~ 68 and ~ 32 at.%, respectively. However, at $U_b = -350$ V, the carbon content decreased by ~ 15 at.%, which gave a film concentration of 53 at.% C and 47 at.% Cr (i.e., C to Cr ratio of nearly 1:1). The decrease in carbon content could be due to the following reasons resulting from high-energy ion bombardment: (1) the continuous and simultaneous dilation process resulting in removal of the less tightly bonded carbon atoms and background gas [24]; (2) resputtering of the weakly bonded carbon adatoms during the coating growth stage [25] due to its small single bond radius of 0.077 nm as compared to 0.125 nm for Cr atom.

3.2. XRD analysis

Fig. 1(a) and (b) shows the glancing angle and $\theta/2\theta$ X-ray diffraction, respectively, of the films deposited at various bias

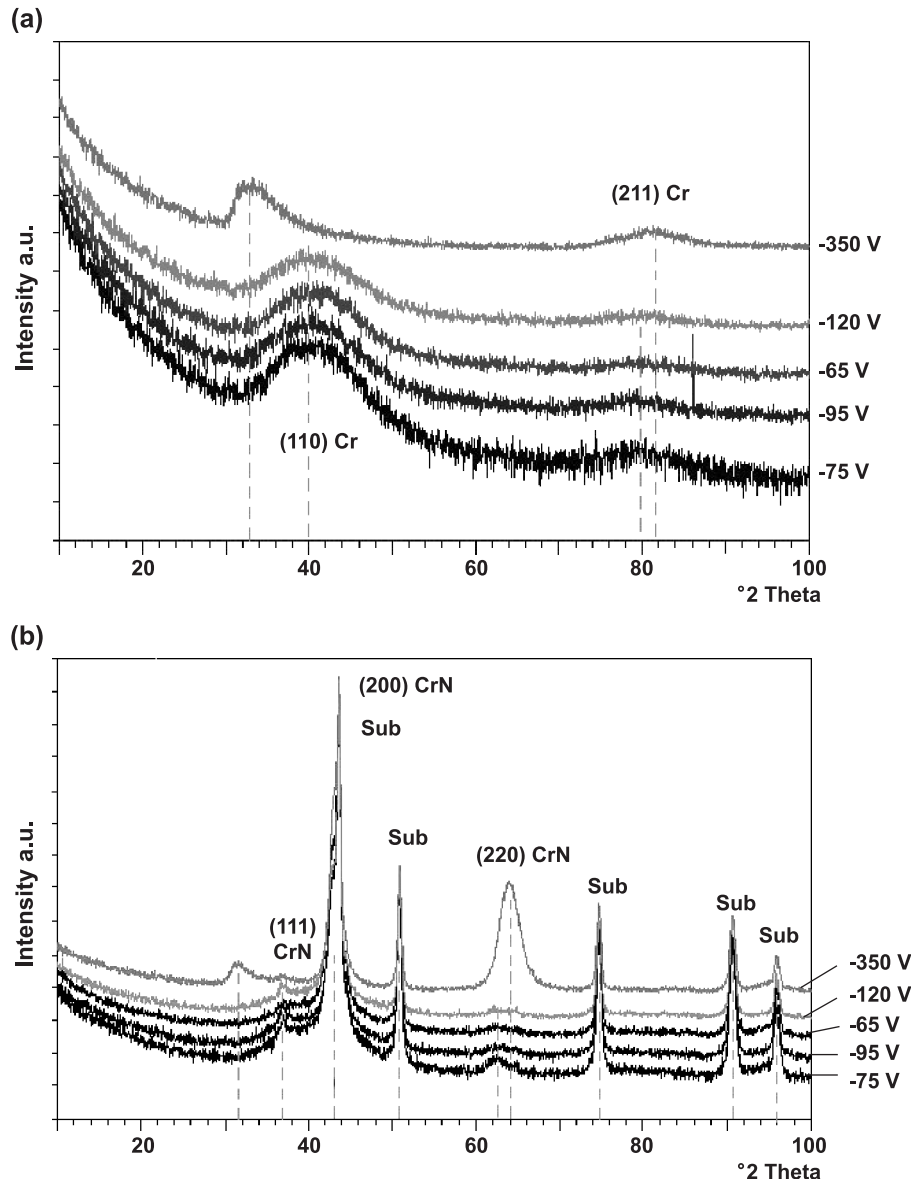


Fig. 1. (a) Glancing angle and (b) $\theta/2\theta$ X-ray diffraction of the films deposited at different bias voltage.

voltages. It was observed that the X-ray diffraction patterns of coatings deposited at U_b between -65 and -120 V were identical. In Fig. 1(a), the absence of the crystalline reflections and the broad diffuse peaks indicates that the film microstructure is essentially amorphous. For U_b between -65 and -120 V, the diffuse peaks appear at 2θ values of $\sim 40^\circ$ and $\sim 80^\circ$ corresponding to the positions of (110) and (211) reflections, respectively, from metallic chromium. At -350 V, the (110) Cr is not present whereas the (211) peak is shifted towards higher angular position. However, a diffuse peak at $\sim 2\theta = 32^\circ$ is present which is close to the (011) Cr_3C_2 reflection. As no other peak corresponding to Cr_3C_2 is present, it is not possible to unambiguously state that the carbide phase has been formed. Fig. 1(b) shows the presence of (111), (200), and (220) peaks from the CrN base layer, which is in agreement with our previous observation [11].

3.3. Microstructure analysis by XTEM and HRTEM

Fig. 2(a) is a bright-field (BF) XTEM image, showing the microstructure of films deposited at $U_b = -350$ V, including the substrate, CrN base layer and the novel multilayer C/Cr coating. Fig. 2(b) and (c) show the near surface region of the films deposited at U_b of -65 and -120 V, respectively, with their corresponding selected area diffraction (SAD) patterns. On all micrographs, carbon appears as the bright region and Cr as the darker region [17,26]. The coating deposited at $U_b = -65$ V is considerably rougher but it becomes smoother and denser as the bias voltage is increased from -65 to -350 V. This is due to the effects of bombardment of the growing films by energetic particles, which enhances the surface mobility of the condensed species, promotes the displacement of surface atoms towards more stable positions in terms

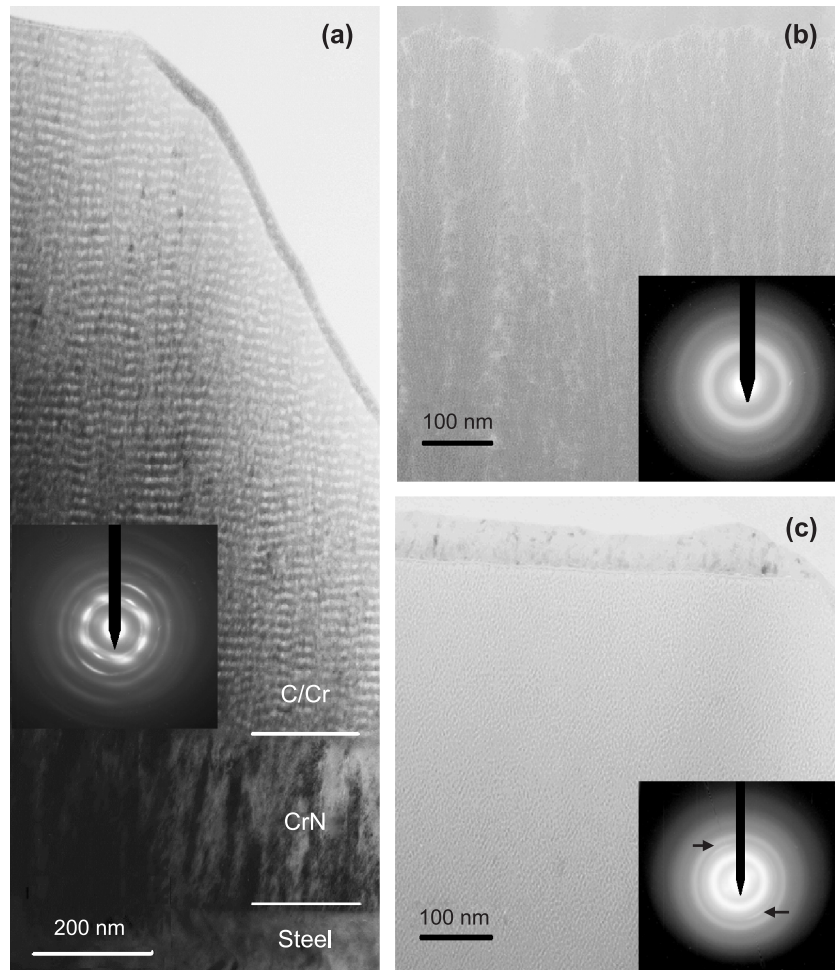


Fig. 2. Bright-field XTEM images showing (a) the architectures of coating deposited at $U_b = -350$ V, and near surface region for (b) $U_b = -65$ V, (c) $U_b = -120$ V, with the corresponding SAD patterns.

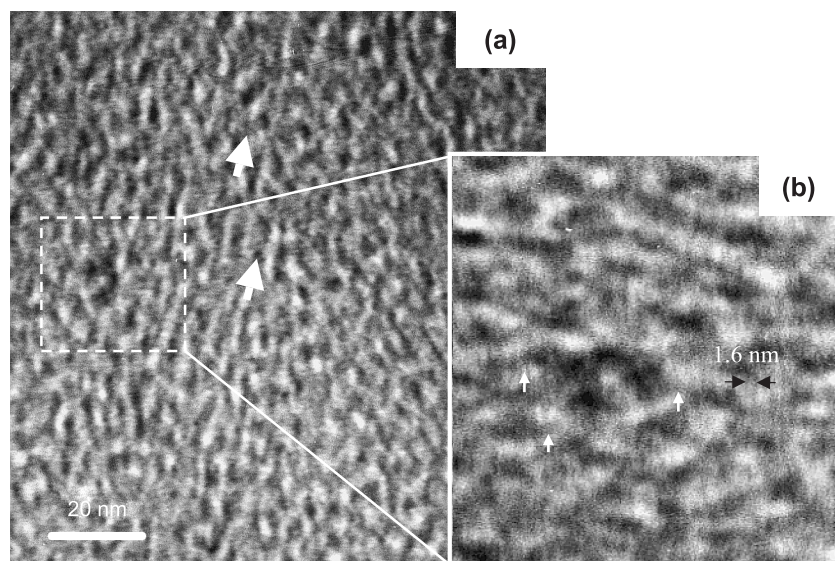


Fig. 3. (a) Higher magnification bright-field images of coatings deposited at $U_b = -120$ V; (b) magnified image of dotted box region (rotated 90° clockwise) showing the artificial multilayer structure (shown by arrows).

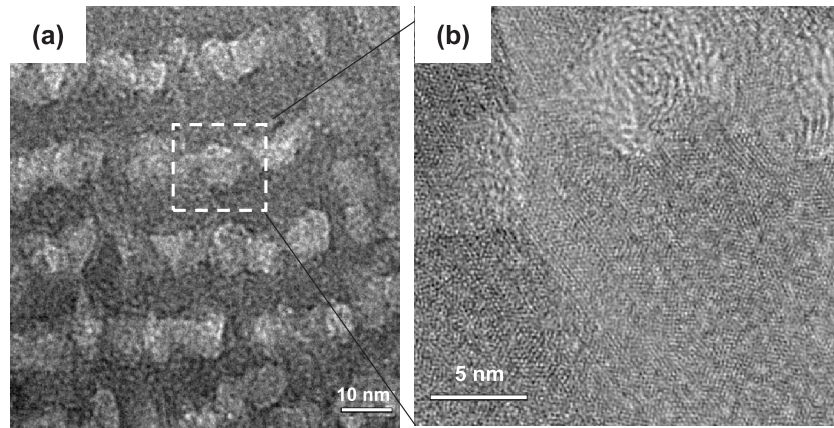


Fig. 4. HRTEM image of the (a) multilayer structure formed at $U_b = -350$ V; (b) magnified image of the nano-onion-like carbon.

of surface energy, and results in the elimination of voids, cavities, and vacancies in the coatings [27]. The coatings deposited between -65 and -95 V show columnar structures with carbon accumulated at the grain boundaries (the white phase between the columns) [17], as shown in Fig. 2(b). However, the width of the column boundaries is markedly reduced as the bias voltage increased from -65 to -95 V (not shown in the figure). This effect is attributed to an increased nucleation probability, accelerating growth and coalescence of the nuclei as the ion energy is increased [16,28,29]. At $U_b = -120$ V [see Fig. 2(c)], the columnar structure transforms to a more uniformly distributed random structure where the number of the onion-like clusters increases both in size and number, the crystallites become slightly aligned in the growth direction [shown by arrows in Fig. 3(a)] as compared to that of U_b between -65 and -95 V. Fig. 3 shows the higher magnification images for $U_b = -120$ V. The artificial multilayer structure with an estimated periodicity of ~ 1.6 nm was highlighted in the dotted box region and included in Fig. 3(b) (the image has been rotated through 90° clockwise to give a better representation of the layer structure). The SAD patterns (Fig. 2 insets) of coating deposited between -65 and -120 V were identical, both showing halo-like diffuse ring patterns, which further revealed the short-range order or amorphous structure of C/Cr coatings. Nonetheless, the crystallinity of the coatings increased with increasing bias voltage, as can be seen by careful observation of the SAD pattern; crystalline diffraction arcs can be seen around the most intense diffuse ring as shown by arrows in Fig. 2(c) (inset). The increased crystallinity of the growing films could be attributed to both

an increase in the kinetic energy of the ions and an increase in the deposition temperature from ~ 260 to ~ 450 °C as a consequence of the increased bias voltage, which increases the surface diffusivity of the adatoms. At -350 V, a rather complex diffraction pattern [Fig. 2(a) inset] was observed, which showed pronounced crystalline reflections from graphitic carbon, chromium crystallites, and chromium carbides (Cr_{23}C_6 , Cr_7C_3 , Cr_3C_2) in the matrix of amorphous carbon. It is obvious that a higher bias voltage of -350 V substantially influences the structure of C/Cr films by affecting the nucleation kinetics, and the degree of preferred orientation of the growing films.

Fig. 4(a) shows the pronounced multilayer structure of the film deposited at $U_b = -350$ V, with an average periodicity of ~ 20 nm which is almost one order of magnitude larger than that for the coatings deposited between -65 and -95 V (bilayer thickness of ~ 2 nm) [17]. The structure comprises of carbon-rich layers (brighter layers segmented in clusters) and chromium-rich layers (darker layers with uniform structure), which are possibly carbides. The carbon layers are built up from the graphite-like carbon which is arranged in nano-onion-like manner, as shown in the magnified image in Fig. 4(b). It can be speculated that the formation of the multilayer structure with the abnormally large bilayer thickness is due to the segregation and self-organisation of the carbon atoms, and possibly the formation of Cr-based carbides, as a result of increased adatom mobility and increased temperature induced by higher-energy ion bombardment. In order to separate the effects of temperature only and increased Cr content, from ion bombardment effects, coatings were also prepared at a higher temperature (400 °C) and at a higher Cr

Table 1
Summarised property of C/Cr coatings

Bias voltage (V)	μ	L_c (N)	Thickness (μm)	Hardness (GPa)	E (GPa)	Stress (GPa)	K_c ($\text{m}^3 \text{N}^{-1} \text{m}^{-1}$)
-65	0.22	48	~ 1.96	8.23	186	0.62	$2.85\text{e}-16$
-75	0.21	75	~ 1.82	11.90	211	1.14	$1.22\text{e}-16$
-95	0.16	70	~ 1.78	17.30	283	1.70	$6.75\text{e}-17$
-120	0.19	50	~ 1.53	19.90	300	2.81	$6.25\text{e}-17$
-350	0.31	20	~ 1.48	25.00	319	2.00	$3.02\text{e}-16$

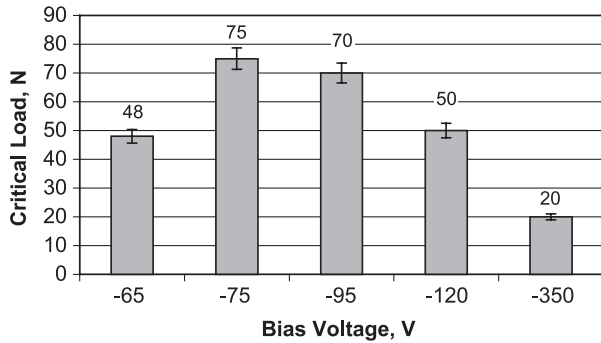


Fig. 5. Critical load as a function of bias voltage.

target power at a bias voltage of -75 V. The transformation from the typical columnar to the distinct multilayer structure could only be observed under conditions of high-energy ion bombardment ($U_b = -350$ V); therefore, the sole influence of high temperature and the high Cr content could be disregarded.

3.4. Mechanical and tribological properties

Table 1 summarises the mechanical and the tribological properties of C/Cr coatings deposited at various bias voltages. The thickness, hardness and the Young's modulus, E , of the

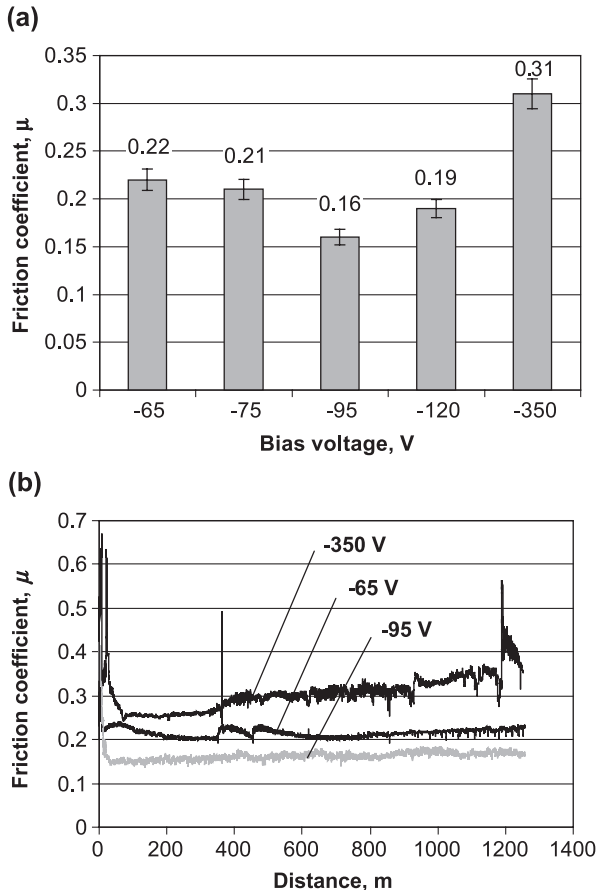


Fig. 6. (a) Friction coefficient and (b) friction curves of C/Cr coatings as a function of bias voltage.

films showed a clear dependence on the substrate bias voltage. An increase in the U_b from -65 to -350 V resulted in decreases in thickness from ~ 1.96 to ~ 1.48 μm , hardness increases from 8.23 to 25 GPa, and an increase in the Young's modulus, E , from 186 to 319 GPa. The stress increased from 0.62 to 2.81 GPa with increasing bias voltage from -65 to -120 V. Further increases in the U_b to -350 V resulted in a reduction in the stress to 2 GPa. The stress values are in good agreement with the levels reported for other carbon-based coatings [30,31]. The decreases in the compressive stress at $U_b = -350$ V could be due to the formation of the layered structure, thermal relaxation of the structure, the enhancement of the adatom mobility which contributes to the relaxation of the compressive stress of the film [30].

Fig. 5 shows the critical load as a function of the bias voltage. The critical load, L_c increased from 48 to 75 N as the bias voltage was increased from -65 to -75 V. Further increase in the U_b to -350 V led to a reduction in the L_c to 20 N. For all the applied bias voltages, no formation of microflakes and spalling of the coatings could be observed inside and at the rim of the scratch, respectively. This demonstrates excellent adhesion between coating and substrate. The pin-on-disc test results shown in Fig. 6(a) demonstrate a clear dependence between the friction coefficient and the bias voltage. The friction coefficient, μ , decreased from 0.22 to 0.16 when the U_b was increased from -65 to -95 V. However, further increases in the U_b to -350 V led to an increase in the friction coefficient to 0.31. The friction curves as shown in Fig. 6(b) become smoother as the bias voltage was increased from -65 to -95 V. It has been reported in our previous work [17] that the coating deposited at -65 V has a rougher surface, larger column diameter which open along column boundaries and crack, thus generating large wear particles during sliding. In addition, the rough surface experiences greater asperity contact, increases tendency to plastic deformation and mechanical interlocking during sliding, resulting in the formation of wear debris, which accumulate in the wear track and promote third-body sliding leading to higher friction and wear coefficients.

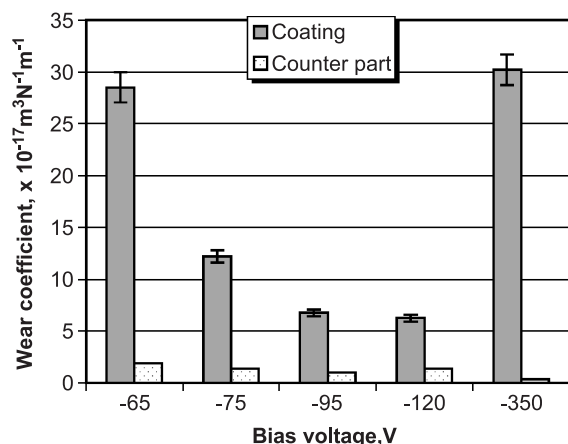


Fig. 7. Wear coefficient as a function of bias voltage.

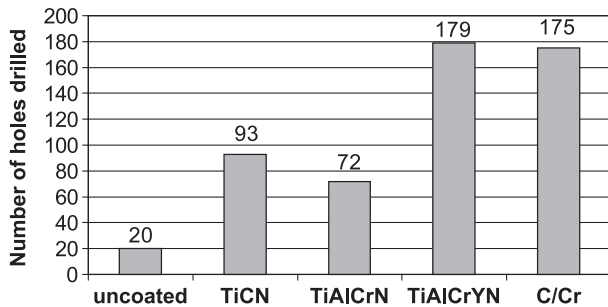


Fig. 8. Number of holes drilled as a function of different coatings.

In contrast, at the higher bias voltage of -95 V, as a result of surface smoothening (less asperity contact) and densification of the coating, sliding wear occurs layer by layer resulting in a lower friction coefficient and a smoother curve. At -350 V, the friction curve becomes rougher and the friction coefficient increases gradually after a sliding distance of ~ 320 m. This could be attributed to the lower carbon content which reduces the lubrication effect, and the high compressive stress in the coating. Fig. 7 shows the sliding wear coefficient of the coatings after pin-on-disc tests. The wear resistant of the coatings correlates well with their friction performance, specifically, films with higher friction coefficient suffer higher wear rates. With increased bias voltage from -65 to -120 V, the wear coefficient of the coatings, K_c , decreased from $\sim 2.8 \times 10^{-16}$ to $\sim 6 \times 10^{-17} \text{ m}^3 \text{ N}^{-1} \text{ m}^{-1}$. However, further increases in the bias voltage to -350 V increased the sliding wear coefficient K_c to $\sim 3 \times 10^{-16} \text{ m}^3 \text{ N}^{-1} \text{ m}^{-1}$.

3.5. Drilling test

Fig. 8 shows the number of holes drilled as a function of different types of coatings. The drilling tests were conducted at a velocity of 38 m/min, with a feed rate of 0.14 mm/rev to a hole depth of 15 mm, using standard HSS drills, 8 mm in diameter coated with C/Cr, using solution treated AISI 304 stainless steel as the work piece material. An improvement of the lifetime by a factor of ~ 9 has been achieved by C/Cr-coated tools as compared to the uncoated tools. In this test, the C/Cr coating outperformed a number of commercially available PVD coatings such as TiCN, TiAlCrN and showed similar performance to TiAlCrYN, a dedicated high-temperature oxidation-resistant coating.

4. Conclusions

The results presented in this paper clearly demonstrate the significant influence of the ion bombardment on the microstructures and the properties of C/Cr coatings:

- High-energy ion bombardment increases adatom mobility and therefore induces surface smoothening, film densification, and nuclei coalescence and enhances the crystallinity of C/Cr coatings.

- The intensive ion radiation in the bias voltage range between -65 and -350 V has promoted segregation and self-organisation of the carbon atoms in the coating.
- C/Cr coatings transformed from the typical columnar structure to a novel multilayer structure with abnormally large bilayer thickness of ~ 20 nm, as the bias voltage increases from -65 to -350 V.
- The structural transformations were found to strongly influence the tribological and mechanical properties of C/Cr coatings.
- Best performance has been achieved with coatings deposited at $U_b = -95$ V ($\mu = 0.16$, $K_c \sim 6 \times 10^{-17} \text{ m}^3 \text{ N}^{-1} \text{ m}^{-1}$), which has a uniformly distributed amorphous structure.

Acknowledgements

Y.N.K. gratefully acknowledges the studentship from Sheffield Hallam University. The authors acknowledge the use of the facilities of the Center for Microanalysis of Materials, which is partially supported by DOE, at the University of Illinois. The authors would like to thank Dr. Stuart Read from Corus R&D, Sheffield UK, for the SNMS analysis, and Tuukka Savisalo from Sheffield Hallam University for hardness and Young's modulus measurements.

References

- [1] M. Grischke, R. Herb, O. Massler, J. Karner, H. Eberle, Society of Vacuum Coaters, 44th Annual Technical Conference Proceedings, 2001, p. 407.
- [2] A. Bloyce, Mater. World (2000 (March)) 13.
- [3] S. Yang, D.G. Teer, Surf. Coat. Technol. 131 (2000) 412.
- [4] S. Yang, D. Camino, A.H.S. Jones, D.G. Teer, Surf. Coat. Technol. 124 (2000) 110.
- [5] A.D. Sarkar, Wear of Metals, Pergamon Press, 1976, p. 137.
- [6] R.H. Savage, J. Appl. Phys. 19 (1948) 1.
- [7] A. Grill, Surf. Coat. Technol. 94–95 (1997) 507.
- [8] F.J. Clauss, Solid Lubricants and Self-Lubricating Solids, Academic Press, 1972, p. 45.
- [9] Y. Liu, E.I. Meletis, J. Mater. Sci. 32 (1997) 3491.
- [10] Y. Liu, A. Erdemir, E.I. Meletis, Surf. Coat. Technol. 94/95 (1997) 463.
- [11] P.Eh. Hovsepian, D.B. Lewis, C. Constable, Q. Luo, Y.N. Kok, W.-D. Münz, Surf. Coat. Technol. 174–175 (2003) 762.
- [12] S. Yang, X. Li, N.M. Renevier, D.G. Teer, Surf. Coat. Technol. 142–144 (2001) 85.
- [13] Y. Liu, A. Erdemir, E.I. Meletis, Surf. Coat. Technol. 86–87 (1996) 564.
- [14] J.E. Greene, S.A. Barnett, J. Vac. Sci. Technol. 21 (2) (1982) 285.
- [15] L. Hultman, U. Helmersson, S.A. Barnett, J.E. Sundgren, J.E. Greene, J. Appl. Phys. 61 (2) (1987) 552.
- [16] Miko Marinov, Thin Solid Films 46 (1977) 267.
- [17] P.Eh. Hovsepian, Y.N. Kok, A.P. Ehiasarian, A. Erdemir, J.-G. Wen, I. Petrov, W.-D. Münz, Thin Solid Films 447–448 (2004) 7.
- [18] W.-D. Münz, F.J.M. Hauzer, D. Schulze, B. Buil, Surf. Coat. Technol. 49 (1991) 161.
- [19] W.-D. Münz, D. Schulze, F.J.M. Hauzer, Surf. Coat. Technol. 50 (1992) 169.

- [20] I. Petrov, P. Losbichler, D. Bergstrom, J.E. Greene, W.-D. Münz, T. Hurkmans, T. Trinh, *Thin Solid Films* 302 (1997) 179.
- [21] C. Schönjahn, L.A. Donohue, D.B. Lewis, W.-D. Münz, I. Petrov, *J. Vac. Sci. Technol., A*, *Vac. Surf. Films* 18 (4) (2000) 1718.
- [22] W.-D. Münz, I.J. Smith, D.B. Lewis, S. Creasey, *Vacuum* 48 (5) (1997) 473.
- [23] J. Albert Sue, “Stress Determination for Coatings”, in *ASM Handbook Vol. 5 Surface Engineering*, The Materials Information Society, 1994, p. 647.
- [24] S. Aisenberg, *J. Vac. Sci. Technol., A*, *Vac. Surf. Films* 2 (2) (1984) 369.
- [25] V.V. Uglov, A.K. Kuleshov, D.P. Rusalsky, M.P. Samzov, A.N. Dementshenok, *Surf. Coat. Technol.* 158–159 (2002) 699.
- [26] N.J.M. Carvalho, J.Th.M. Dehossou, *Thin Solid Films* 388 (2001) 150.
- [27] N. Maréchal, E. Quesnel, Y. Pauleau, *J. Mater. Res.* 9 (7) (1994) 1820.
- [28] M. Ohring, *The Materials Science of Thin Films*, Academic Press, Boston, 1992.
- [29] M. Odén, C. Ericsson, G. Håkansson, H. Ljungcrantz, *Surf. Coat. Technol.* 114 (1999) 39.
- [30] X.L. Peng, T.W. Clyne, *Thin Solid Films* 312 (1998) 207.
- [31] B.K. Gupta, Bharat Bhushan, *Thin Solid Films* 270 (1995) 391.